Catena 118 (2014) 206–219

Contents lists available at ScienceDirect

Catena

journal homepage: www.elsevier.com/locate/catena

Effects of climate change and wildfire on soil loss in the Southern Rockies Ecoregion

S.E. Litschert [a,*,1], D.M. Theobald [b,2], T.C. Brown [c]

[a] Warner College of Natural Resources, Colorado State University, Fort Collins, CO 80523, United States
[b] Dept. of Fish, Wildlife, and Conservation Biology, Colorado State University, Fort Collins, CO 80523, United States
[c] Rocky Mountain Research Station, U.S. Forest Service, Fort Collins, CO 80526, United States

ARTICLE INFO

Article history:
Received 21 March 2013
Received in revised form 12 January 2014
Accepted 19 January 2014
Available online 18 February 2014

Keywords:
Climate change
Soil loss
Wildfire
Erosion
RUSLE
Southern Rockies Ecoregion

ABSTRACT

Forests in the Southern Rockies Ecoregion surround the headwaters of several major rivers in the western and central US. Future climatic changes will increase the incidence of wildfire in those forests, and will likely lead to changes in downstream water quality, including sediment loads. We estimated soil loss under the historic climate and two IPCC climate change emissions scenarios (A2 and B1); each scenario was modeled using statistically downscaled climate data from global circulation models (GCMs; ECHAM5 and HadCM3) for each of thirteen land cover types. We used the Revised Universal Soil Loss Equation (RUSLE) and developed a way to calculate rainfall erosivity, a key factor in RUSLE, to account for climate change. We also incorporated the effects of climate change on wildfire to create stochastic spatial distributions of wildfires and to inform changes in land cover. Based on 100 simulations of future wildfire applied to RUSLE for each GCM-scenario combination, we found that soil loss will likely increase above historic levels but that considerable uncertainty remains about the amount of increase. Across the GCM-scenario combinations, mean soil loss increased above historic levels by from 3% (HadCM3-A2) to 65% (ECHAM5-B1) for climate change only and the effects of wildfire increased soil loss an additional 3 to 5%.

1. Introduction

The effects of increased erosion and sedimentation on aquatic ecosystems including fish habitat, channel morphology, and municipal water supplies are critical issues in many watersheds (e.g. EPA, 2000; MacDonald and Stednick, 2003; Shaw and Richardson, 2001; Troendle and Olsen, 1994). Sediment is probably the most important water quality concern (EPA, 2000), as increased sediment raises the cost to treat and supply domestic water, reduces reservoir storage, and increases reservoir maintenance needs (Graham, 2003; Palmieri et al., 2001). Further, several other pollutants preferentially bind to fine sediment particles, which may be transported downstream, degrading the quality of raw water supplies (EPA, 2000). In the western United States, 65% of the water supply originates on forested watersheds (Brown et al., 2008) and the Southern Rockies Ecoregion (SRE) provides the headwaters to many of the rivers that supply this water.

Climate change, which will affect precipitation, temperature, and land cover, is likely to strongly influence the processes causing surface erosion. Surface erosion is the removal and transportation of soil by raindrop impact and overland flow (Foster and Meyer, 1977; Wischmeier and Smith, 1978). These processes are driven by rainfall intensity and amount, and are modified by topography, soil and land cover types. In the western US, projected increases in temperature and changes in precipitation (Ray et al., 2008) will likely affect both erosion and wildfire in the SRE. When temperatures increase, more precipitation falls as rain (instead of snow) and extreme rainfall events become more likely (IPCC, 2007). The increase in the amount and intensity of rain is the dominant process most likely to increase erosion (Nearing, 2001).

The length of fire seasons and extent of annual burned area are strongly related to seasonal changes in precipitation and temperature (Balshi et al., 2009; Bartlein et al., 2003; Littell et al., 2009; Westerling et al., 2006). Burned area is significantly and positively correlated with spring and summer temperatures (Littell et al., 2009). Summer and autumn precipitation control fuel moisture (Drever et al., 2009; Littell et al., 2009; Westerling et al., 2006). In the southwestern US, climate models consistently project increased temperatures for the 21st century but disagree about the amount of future precipitation. Increases in temperatures are likely, aside from any change in precipitation, to expand the total area burned by wildfires worldwide (IPCC, 2007), in north America (Drever et al., 2009; Spracklen et al., 2009; Westerling et al., 2006), and in the SRE (Litschert et al., 2012).

Wildfires in the SRE burn with varying severity and can result in decreased vegetation cover, the conflagration of organic material such as leaf litter, development of hydrophobic soils, and soil sealing (DeBano, 1981; Larsen et al., 2009). The removal of organic material

* Corresponding author.
E-mail address: sam@earthsystems.net (S.E. Litschert).
[1] Present address: Earth Systems Institute, Fort Collins, CO 80521.
[2] Present address: Conservation Science Partners, Fort Collins, CO 80524.

0341-8162/$ – see front matter © 2014 Elsevier B.V. All rights reserved.
http://dx.doi.org/10.1016/j.catena.2014.01.007

that previously absorbed precipitation leads to increased surface erosion, in some cases by several orders of magnitude as compared to undisturbed areas, as rain splash causes detachment or entrainment of sediment (Moody and Martin, 2001; Neary et al., 2005). Similarly, hydrophobic soils reduce infiltration because moisture may not penetrate the hydrophobic layer (DeBano, 1981). Precipitation on bare mineral soils, exposed by wildfires, converges as overland flow that causes further erosion in the form of rills and gullies that may connect to streams, increasing downstream sedimentation. In summary, climate change will likely affect precipitation, land cover, and fire regimes; hence it is important to consider these effects on potential changes in erosion.

In recent years, climate modeling for the western US has been refined to include key factors such as the El Nino-Southern Oscillation (ENSO) and the Pacific Decadal Oscillation (PDO) (Cañon et al., 2007, 2011). In a test of 16 global circulation models (GCM), HadCM3 and ECHAM5 were considered the best for simulating climate in the southwestern US (Dominguez et al., 2010). Improvements in downscaling global circulation model (GCM) output have resulted in data that can be used as input into watershed scale hydrologic and sediment models (e.g. Cañon et al., 2011; Hay et al., 2000; Wood et al., 2004). Hence, hydrologic and sedimentary changes for future climate conditions can be estimated using the downscaled climate data.

Given that strong temperature and precipitation gradients in this mountainous region dictate patterns of land cover type, our goal for this study was to calculate future soil loss for different land cover types across the SRE using projected changes in climate and wildfire extent. The underlying objective was to provide land managers with a quantitative assessment of changes in soil loss and of the uncertainty associated with soil loss changes in the future. To achieve this goal we: (1) used a burned area model to estimate the extent of future wildfires and to stochastically generate and map future wildfire events (Litschert et al., 2012); (2) combined the resulting wildfire maps with broad land cover types; (3) estimated spatial patterns of rainfall erosivity for historic and projected climates; and finally (4) used the modified land cover and rainfall erosivity layers to estimate soil loss using the Revised Universal Soil Loss Equation (RUSLE) for each of thirteen land cover types. In RUSLE, soil loss is a product of values for rainfall erosivity, soil erodibility, slope length and gradient, land cover, and agricultural practices (Renard et al., 1997). We computed soil loss for a past time period (1970–2006), and for two future time periods (2010–2040 and 2040–2070) for each of four sets of downscaled climate data corresponding to two Intergovernmental Panel on Climate Change (IPCC) global emissions scenarios (A2, B1) each modeled using two GCMs (ECHAM5 and HadCM3).

2. Site description

The SRE (Bailey et al., 1994) consists of almost 144,000 km^2 of generally mountainous terrain in central Colorado, southern Wyoming and northern New Mexico, ranging in elevation from 1000 to 4400 m. The SRE is of critical importance for water supply as it contains the headwaters of the Colorado, Platte, Arkansas, Rio Grande, and Canadian Rivers (Fig. 1). Mean annual precipitation (1971–2000) ranges from 170 mm at the lower elevations to 1600 mm at the highest elevations. Mean annual temperatures for 1970–2000 range from −4° to 13 °C at highest to lower elevations respectively. Vegetation in the SRE includes prairie, shrub lands, and pinyon–juniper woodlands at the lower elevations; ponderosa pine, lodgepole pine and sub-alpine fir at the mid and higher elevations; and alpine tundra at the highest elevations.

3. Methods

We estimated average annual soil loss using RUSLE (Renard et al., 1997) in ESRI™ ArcGIS 9.2 using Python 2.4. Because we wanted to provide information to land managers about potential changes in soil

Fig. 1. The Southern Rockies Ecoregion (SRE) showing the sources of several major rivers and surrounding states.

loss and sedimentation due to climate change, we needed to select an approach that was appropriate for modeling changes over large areas. RUSLE is a relatively simple and computationally efficient model well suited for modeling changes at the broad, landscape level. Using RUSLE, we were able to examine nine historic and future data combinations across the SRE, each of which was implemented 100 times. The use of a more detailed, physically based model was impractical over such a large and heterogeneous area as the SRE (e.g. Caminiti, 2004; Merritt et al., 2003). Despite its origins in agriculture, RUSLE has been used to calculate soil loss in a variety of other land cover and topographic types, including forested watersheds (e.g. Breiby, 2006; Gonzalez-Bonorino and Osterkamp, 2004; Toy and Foster, 1998). We next describe how we parameterized the six factors of RUSLE, calculated soil loss for climate change and wildfire combinations, and analyzed the RUSLE output.

3.1. Parameterizing RUSLE

In RUSLE, the rate of annual soil loss (A; Mg ha^{-1} yr^{-1}) is the product of six factors:

$$A = R \times K \times L \times S \times C \times P \tag{1}$$

where R is annual rainfall erosivity (MJ mm ha^{-1} h^{-1} yr^{-1}), K is soil erodibility (Mg ha h ha^{-1} MJ^{-1} mm^{-1}), L is slope length, S is slope gradient, C is land cover, and P is agricultural practices (Renard et al., 1997). L, S, C, and P are dimensionless. We calculated A for a two-dimensional surface of the SRE represented by a raster with cells identified with coordinates (i,j). We implemented RUSLE at a spatial

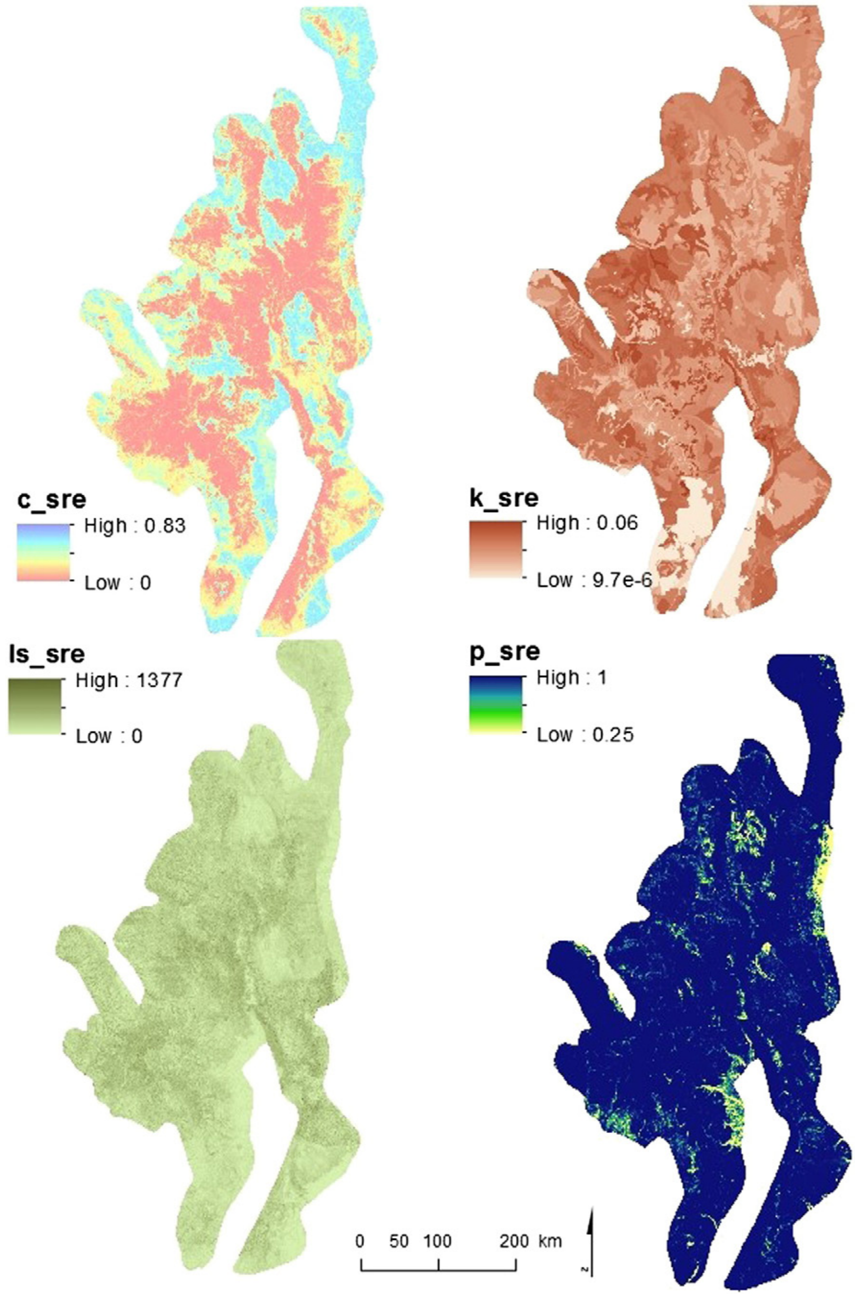

Fig. 2. RUSLE base layers for land cover (C), soil erodibility (K), length-slope (LS), and agricultural practices (P). Rainfall erosivity (R) is in Fig. 5.

resolution (cell length) of 2 km and base layers are shown in Fig. 2. As explained below, we modified rainfall erosivity using predicted precipitation and temperature values in order to account for the effects of climate change.

3.1.1. Rainfall erosivity

The rainfall erosivity factor (R) was originally computed by summing the products of the energy and intensity from qualifying rainfall events (Renard et al., 1997). Because rainfall energy and intensity are difficult to measure, especially over large areas, the rainfall erosivity factor has been modeled as a function of mean annual precipitation (*MAP*; Renard and Freimund, 1994), as follows:

$$R_{i,j} = 0.04830 * MAP_{i,j}^{1.61} \quad \text{where } MAP <= 850 \text{ mm} \tag{2a}$$

$$R_{i,j} = 587.8 - 1.219 * MAP_{i,j} + 0.004105 * MAP_{i,j}^{2} \quad \text{where } MAP > 850 \text{ mm}. \tag{2b}$$

The downscaled GCM data[3] that we used from ECHAM5 and HadCM3 did not show a clear trend for precipitation in the SRE (Litschert et al., 2012; Fig. 3). In contrast to the lack of precipitation trends, temperature projections show increases of 2–3 °C by 2070. Temperature changes of this magnitude are likely to alter the precipitation regime (e.g. Barnett et al., 2005; Feng and Hu, 2007; IPCC, 2007; Nijssen et al., 2001); the distinction between precipitation as rain or snow is critical because rain generally causes more erosion than snow (Renard et al., 1997). Although runoff from snow may cause minor amounts of erosion, we do not consider that process here.

[3] Climate data were obtained in 2008 at http://www.sahra.arizona.edu/research_data/SAHRAGeoDB.

Cooley et al. (1988) reviewed detailed temperature and precipitation data for Reynolds Creek Experimental Watershed (RCEW) in southwestern Idaho and found that a mean monthly temperature of 1 °C was the threshold between a snowfall dominated month and a rainfall dominated month. Climate data (n = 45 years) at the site indicate that it is responding to climate change as the SRE is expected to respond, i.e. an increase in temperature and no consistent trend in the amount of precipitation (Nayak et al., 2010). Alternately, Nayak et al. (2010), in a more quantitative study using climate data for RCEW, assumed that if the dew point temperature was greater than 0 °C, rain fell; if the temperature was less than zero, snow fell, and if "close to 0 °C", precipitation fell as mixed rain and snow. We used Cooley's threshold of 1 °C because rain-on-snow events are rare in the SRE and because it is the more conservative approach for determining erosivity. The dynamics of determining precipitation phase are complex and phase may vary with individual weather patterns, latitude, and topography; our objective was to find a regional value that could be generalized to the SRE at a broad scale.

Downscaled GCM data at a cell size of 2 km were available for the four seasons: winter (January, February, March); spring (April, May, June); summer (July, August, September); and autumn (October, November, December). Using the assumption that seasonal precipitation would fall as snow if the temperature was less than or equal to 1 °C and fall as rain otherwise (Cooley et al., 1988), seasonal rainfall averages were summed to calculate mean annual rainfall, which was used in Eqs. (2a)–(2b) in place of mean annual precipitation. We did not account for the effects of rain-on-snow events, which are rare in the SRE, or for frozen ground.

To evaluate the accuracy of the rainfall erosivity layer produced using Eqs. (2a)–(2b), we visually compared the layer for the historic period (1970–2006) with the rainfall erosivity layer developed by the Environmental Protection Agency (EPA).[4] For input to Eqs. (2a)–(2b) we used climate data from PRISM[5] (Daly et al., 1994). The EPA rainfall erosivity layer is a function of measured rainfall intensity and topographic data, and is the only other example of raster-based rainfall erosivity that we could find; we could not use it for projections because it does not account for rainfall erosivity under any climate change scenarios. We refer to these layers as historic R_{RF} (Renard and Freimund, 1994) and R_{EPA} rainfall erosivity, respectively. We then calculated rainfall erosivity layers for each of the climate-scenario-time-period combinations using the downscaled GCM data and Eqs. (2a)–(2b). We calculated the changes in rainfall erosivity from historic to future time periods for each land cover type.

3.1.2. Soil erodibility

The soil erodibility factor (K) is a measure of how soil properties affect soil loss. We used spatial data representing the K-factor, resampled to 2 km cell size, from the National Resources Conservation Service.[6] We assumed that soil erodibility would remain static over the relatively short time period modeled in this study, and thus that climate change would not affect K. Similarly, the K-factor was not altered to account for the effects of wildfires. Wildfires, particularly high severity burns, are known to affect soil texture, structure, organic content, and hydrophobicity (e.g. DeBano, 1981, 2000; Huffman et al., 2001; Moody and Martin, 2001; Neary et al., 2005; Robichaud, 2000). However, insufficient data exist to quantify these effects adequately (Larsen et al., 2009).

3.1.3. Length-Slope

The Length-Slope (LS) factor accounts for how topography affects soil loss (Renard et al., 1997). We calculated the length-slope factor at the 30 m cell size using data from the US Geological Survey[7] and resampled to 2 km cell size for use in RUSLE calculations.

A slope factor (S) is a component of the LS factor. Nearing (1997) provides a single continuous function for S that can be applied to slopes up to 55%, whereas previous functions fit slopes up to only 22% (McCool et al., 1987). Nearing's equation is:

$$S_{i,j} = -1.5 + \frac{17}{1 + e^{\left(2.3 - 6.1 * \sin\beta_{i,j}\right)}} \tag{3}$$

where $S_{i,j}$ is the slope factor and $\beta_{i,j}$ is the mean slope angle in radians. Slopes higher than 55% were limited to 55% since extrapolation beyond the limit of Nearing's empirical equation could result in more uncertainty and exaggerate soil erosion values.

We calculated the LS factor using Winchell's method (2008):

$$LS_{i,j} = S_{i,j} * \frac{\left(A_{i,j-in} + D^2\right)^{m+1} - A_{i,j-in}^{m+1}}{D^{m+2} * x_{i,j}^{m} * (22.13)^{m}} \tag{4}$$

where $A_{i,j}$ is the contributing area to cell i,j; D is the cell size (m); $x_{i,j}$ is the aspect direction; and m is the slope length exponent. m is given by:

$$m = \frac{\beta}{1+\beta} \tag{5}$$

where

$$\beta = \frac{\sin\vartheta_{i,j} / 0.0896}{3 * \sin\vartheta_{i,j}^{0.8} + 0.56} \tag{6}$$

and $\theta_{i,j}$ is the slope in degrees. The LS-factor was held constant throughout all RUSLE simulations as topography at this coarse resolution is unlikely to change substantially in the time being modeled.

3.1.4. Land cover

To generate a base land cover layer, we began by broadly categorizing cells as vegetation, roads, or developed areas based on merging data from LandFire existing vegetation (EVT; LandFire, 2006) and roads data from ESRI Street Map[8] and, for unpaved roads, the US Forest Service.[9] We grouped EVT data into 13 broad land cover types: alpine tundra (AT), high elevation forest (HEF), mid-elevation forest (MEF), low elevation forest (LEF), lodgepole pine (LP), shrub/grassland (ST), riparian/wetland (RW), barren/water/snowfield (BWS), agriculture irrigated crops (ACI), agriculture/open space (AOS), high intensity developed (HID), mid intensity developed (MID), low intensity developed (LID). Land cover (C) factor values for each land cover type were obtained from the literature and the percent area covered by each land cover type was calculated using the LandFire data (Table 1). The most prevalent land cover type is shrub/grassland (30%), closely followed by different forest types. Developed areas were least prevalent in the SRE comprising only 0.67%.

In the base land cover layer, if a road passed through a cell, that cell was categorized as road. We classified roads as highways and interstates, other paved roads, gravel roads, and unpaved roads based on US Forest Service Feature Class Codes (FCC) and Street Map Cartographic Feature File (CFF) codes (Table 2). Road cells were comprised of a variety of land cover types: impervious cover, grass, soil, and gravel. We used the American Association of State Highway and Transportation Officials (AASHTO) guidelines of road, median, and shoulder widths to calculate the percentage of each land cover that comprised each road type of each cell (AASHTO, 2004). We determined the land cover factors from the literature for each land cover type in a road cell (Table 2). We calculated an area-weighted land cover factor using the product of percent

[4] http://www.epa.gov/esd/land-sci/emap_west_browser/EMAP-West_Metric_Browser.htm. Accessed 2009.

[5] PRISM Climate Group, Oregon State University, http://prism.oregonstate.edu, created 4 Feb 2004.

[6] STATSGO; http://soils.usda.gov/survey/geography/statsgo/, Accessed 2009.

[7] National Elevation Data; http://ned.usgs.gov/, Accessed 2009.

[8] http://www.esri.com/data/free-data. Accessed 2009.

[9] http://fsgeodata.fs.fed.us/vector/index.php. Accessed 2009.

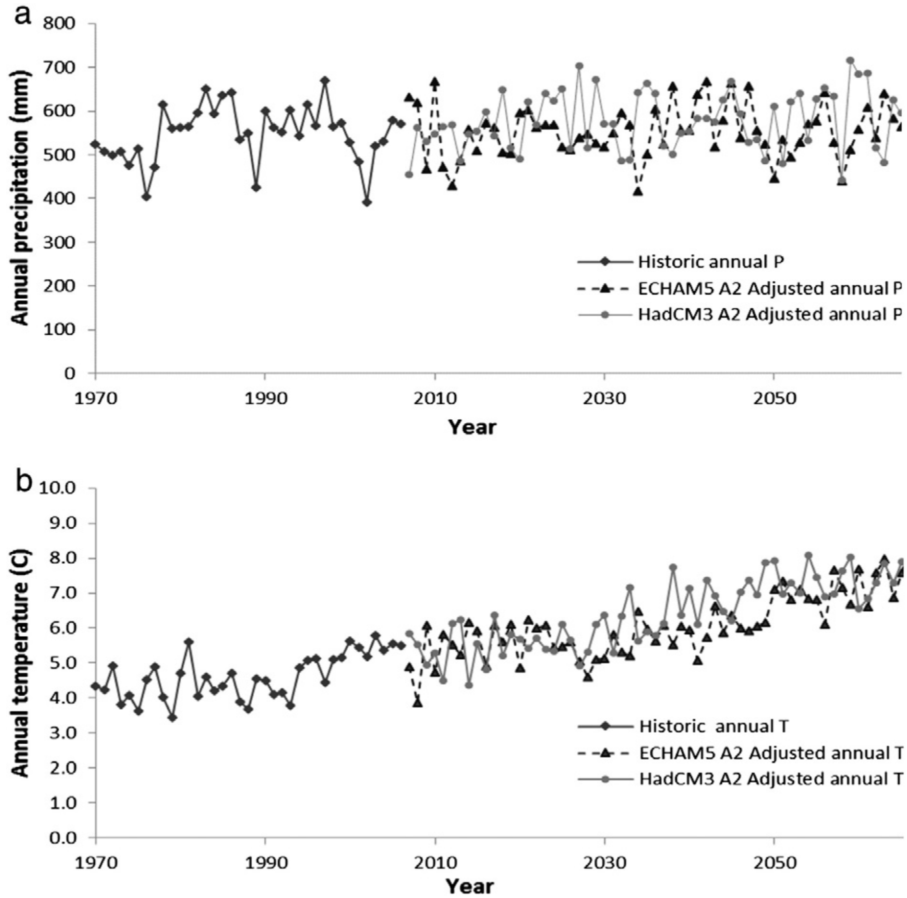

Fig. 3. Historic and projected annual precipitation and temperature for the SRE. Historic data are from PRISM and projected data are from two GCMs and emission scenario A2 (from Litschert et al., 2012).

area of impervious surface, grass, soil, and gravel with their respective land cover values to adjust standard road surface for each road type to a 30 m cell based on standard road widths (Table 2).

The land cover layer, generated from the base land cover layer using values from Tables 1 and 2, was used without the burned area modeling to calculate soil loss due to climate change only. To calculate the combined effects of climate change and wildfire, burned areas were assigned to land cover layers. *C* values for roads superseded vegetation and developed areas, and *C* values for wildfires superseded all other land cover types. Potential changes in vegetation type due to the changing climate were not accounted for due to the lack of data.

We used the Burned Area model (BAM) to project the extent of annual burned areas (BA) in the SRE for incorporation into a land cover layer (Litschert et al., 2012). BAM uses variables obtained from downscaled GCM data for summer precipitation (SumP), previous autumn precipitation (PAutP), five year previous precipitation (P5P) and five year previous temperature (P5T):

$$BA = -4.166 - 0.008 * SumP - 0.010 * PAutP + 0.003 * P5P + 0.421 * P5T. \tag{7}$$

Litschert et al. (2012) evaluated the predictive accuracy of three burned area models, developed with the same dataset, using ten-fold cross-validation. The BAM used in this study (called the Combined Model in Litschert et al., 2012) scored the best in the cross-validation test. We further evaluated the BAM by obtaining new fire data for years 2007–2011 from the US Forest Service and climate data from

Table 1
Land cover factor (C) for vegetation and developed areas with codes, descriptions, and sources.

Land use code	Land cover factor	Reference	Description in reference
High elevation forest	0.002	Breiby (2006)	Coniferous forest
Low elevation forest	0.0928	Miller et al. (2003)	Pinyon–juniper
Lodgepole pine	0.002	Breiby (2006)	Coniferous forest
Mid elevation forest	0.0027	Miller et al. (2003)	Ponderosa pine
Riparian/wetland	0.0005	Miller et al (2003)	Aspen
Shrub/grass	0.227	Miller et al. (2003)	Plains grassland
Agriculture irrigated crops	0.24	McCuen (1998)	Agriculture irrigated crops
Agriculture/open space	0.14	McCuen (1998)	Pasture hay
Alpine tundra	0.0001	Dawen et al. (2003)	Snow field
Barren/water	0	Breiby (2006), McCuen (1998)	Open water, exposed rock
Developed urban	0.001	Guobin et al. (2006)	Developed urban
Developed general	0.003	Guobin et al. (2006)	Developed general
Developed suburban	0.002	Guobin et al. (2006)	Developed suburban

Table 2
Land cover factor values for different road types which are typically comprised of up to four land cover types. The land cover factor calculated for each road type is the sum of each area weighted land cover value (bottom line).

Road type	Total foot print (meters)	% impervious	% grassland	% bare soil	% gravel	Land cover factor calculated for road cell	USDA Forest Service Feature Class Codes (FCC)	ESRI streetmap cartographic feature file
U.S. highways & interstates	60	0.75	0.1	–	0.15	0.03		A1, A2
Paved roads	30	0.86	0.14	–	–	0.03		A3–A7, excluded FCC codes for gravel and dirt
Gravel roads	30	–	0.05	0.05	0.9	0.1	94,518	
Unpaved roads	30	–	0.1	0.9	–	0.83	89,95,515	
Land cover value used in calculation		0.0001[a]	0.227[b]	0.9[b]	0.05[b]			

[a] We assumed a very low value for impervious to avoid zero errors in calculations.
[b] Source of land cover values: grassland (Miller et al., 2003); bare soil (Haan et al., 1994 (After Israelson et al., 1980)); gravel (Wischmeier and Smith, 1978).

Table 3
Fire size classes with historic numbers of fires and summary of fire areas used to develop fire distributions and GIS layers (see text for more detail).

Fire size class	A	B	C	D	E	F	G
Fire class area (km^2)	<0.001	0.001–0.004	0.04–0.40	0.40–1.2	1.2–4.0	4.0–20.2	>20.2
Numbers of fires (1971–2006)	10,027	4318	466	91	43	24	22
Percent of burned area (1971–2006)				4.9	4.5	12.8	74.2
Mean fire area (km^2)				0.71	2.1	11	97
Max fire area (km^2)				1.2	4.2	18	557
Max fire radius (km^2)				0.618	1.16	2.39	13.32

PRISM; both data sources were the same as those used to develop the BAM. The total annual burned area for 2007–2011 ranged from 0.03% to 0.60% of the SRE which is within the range of annual burned area values used to develop the BAM. The average difference in total burned area (of the Southern Rockies Ecoregion) between real and modeled data over the five year period was 3% with slightly larger annual variations. We conclude that the BAM is adequate to model mean annual percent burned area for future climate projections as used in this manuscript.

Annual burned area predicted by BAM is the sum of area burned in the following vegetation types: low, mid, and high elevation forest including lodgepole pine, riparian vegetation, and steppe/shrub; because of fire data limitations, the BAM does not distinguish between vegetation types. The BAM projects amount of burned area only; it does not provide fire ignition points or information about burn severity (Litschert et al., 2012). Thus, for this study we developed procedures to locate fires and specify a fire's burn severity.

To locate or distribute the projected burned area across the landscape, we generated lists of fires by size and number that matched the historic distribution for each US Forest Service designated fire size class (Table 3) and that summed to the modeled burned area total. Using the list of numbers of fires, we generated GIS layers with each

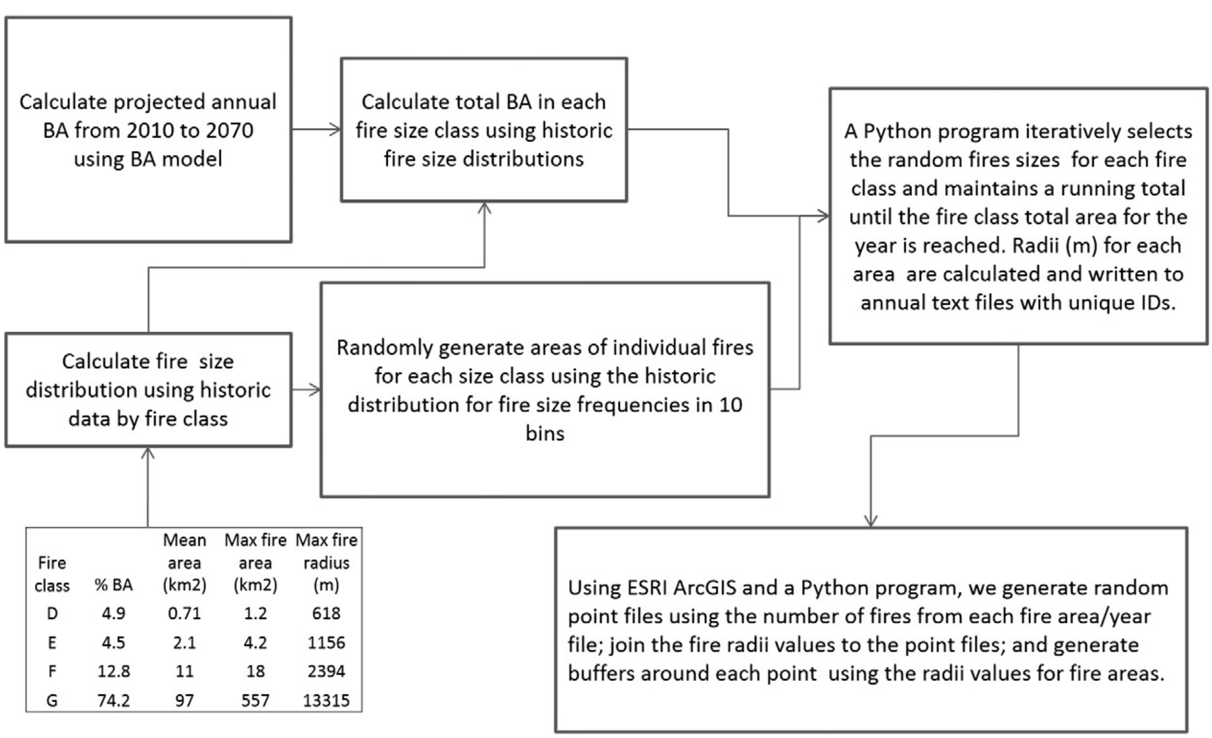

Fig. 4. Details of the process to generate annual burned area (BA) GIS layers using historic fire distributions and climate data for each emission scenario (A2, B1)—GCM (ECHAM5, HadCM3) combination.

Table 4
Land cover factor for burned areas by vegetation type and burn severity.

Burned vegetation type	Land cover factor for low/mixed fire severity	Land cover factor for stand replacing fire severity	Vegetation type in reference	Reference
Riparian/wetland	0.0016	0.07	Aspen	Miller et al. (2003)
Shrub/grassland	0.392	–	Plains grassland	Averaged values in Miller et al. (2003)
Low elevation forest	0.178	0.2402	Pinyon–juniper	Miller et al. (2003)
Lodgepole pine, mid elevation forest, and high elevation forest	0.052	0.207	Ponderosa and lodgepole pine	Average: Miller et al. (2003), Larsen and MacDonald (2007)

fire represented by a randomly placed circle that corresponded to the fire area. We ran the simulations by decreasing fire size class (i.e. we simulated larger fires first) and masked already burned area so that burned areas did not overlap. We then merged fires for all fire size classes to create one burned area iteration layer. A detailed flowchart of this process is in Fig. 4.

Using BAM, we stochastically generated 100 burned area layers as described above for each combination of climate model, emission scenario, and future time period, yielding eight sets of 100 fire layers each. In addition, we produced 100 burned area layers for the historic climate and time period for a total of 900 fire layers for the SRE.

Burn severity, which typically varies by vegetation type (Kilgore, 1981), was incorporated into the burned areas by overlaying each burned area layer with the Fire Regime Group (FRG) data from Landfire (2006). FRG represents fire severity in three classes: low (surface litter is partially consumed); mixed (litter layer is consumed); and stand replacing (surface litter and organic matter are burned, soil is disaggregated, and soil chemistry is altered). The low and mixed fire severity classes were combined to determine burn severity as we did not have land cover values for both classes separately. Once the fire severity for each burned cell was obtained, rasters were generated where burned cells were assigned land cover factors for each vegetation type and burn severity class. As with unburned areas, the land cover factors were taken from the literature (Table 4). For example, a cell representing an area of lodgepole pine, which would burn with stand-replacing severity, was assigned a land cover factor of 0.207 (Table 4).

We merged the land cover layer generated for each burned area and burn severity iteration with the base land cover layer to generate 900 land cover layers. Note that because data were lacking, the BAM process did not account for wind speed, wind direction, topography, or fire spread. The BAM did not account for vegetation recovery after the fire because we ran the burned area layers as independent, worst-case scenarios.

3.1.5. Crop management factor

The crop management factor (P) in RUSLE varies by agricultural practice and slope; P is used only in areas of cultivated crops. Due to the lack of detailed crop data, we calculated the average of P values for contour, strip crop, and irrigated furrows (Dunne and Leopold, 1978) for slope ranges 2–7%, 8–12%, 13–18%, and 19–24% (Table 5). For areas that were not used as cropland, the P value was assigned to 1 as this would have no effect on the calculation of RUSLE. For any given location, P was the same for each combination and did not vary over time, and thus had no effect on soil loss differences.

Table 5
Crop management (P) factor values averaged for agricultural management practices and calculated by slope ranges (Dunne and Leopold, 1978).

Slope %	P-factor
2–7	0.25
8–12	0.3
13–18	0.4
19–24	0.45

3.2. Running RUSLE simulations and analyses

Soil loss was calculated using data from historic climate records (1970–2006) and two spatially downscaled GCMs (HadCM3, ECHAM5). Data from each downscaled GCM were obtained for two IPCC emission scenarios (A2, which projects high increases in temperature, and B1, which projects lower temperature increases; IPCC, 2007) and for two time periods (T1 = 2010–2040, T2 = 2041–2070), resulting in eight different future combinations of climate, scenario, and time period. Further, we ran simulations with and without wildfire, for a total of 18 combinations.

We used ANOVA to test for differences in soil loss among the 18 combinations of downscaled climate data, climate scenarios, time period, and wildfire. The Tukey Honestly Significant Difference test (HSD; Ott and Longnecker, 2001), a conservative multiple comparison test, was used to determine which pair-wise comparisons of the nine combinations of climate, scenario, and time period with fire were significantly different from others. The R statistical package was used for all statistical analyses (R. Development Core Team, 2011. Version 2.13.1).

We calculated soil loss for each land cover type for the historic and future time periods. We compared these changes across downscaled GCMs, climate scenarios, time periods using the percent change in soil loss from historic to future time periods. Wildfire was not included in this part of the analysis since the BAM did not differentiate between land cover types.

We selected a raster of median soil loss from among the 100 iteration datasets for each of the following conditions: (1) the historic climate, (2) the future combination with the highest soil loss (EB1T1), and (3) the future combination with soil loss closest to the mean change in future soil loss from the historic (HB1T2). We visually compared cumulative density plots of these three median rasters and calculated probabilities for differing amounts of soil loss under these combinations.

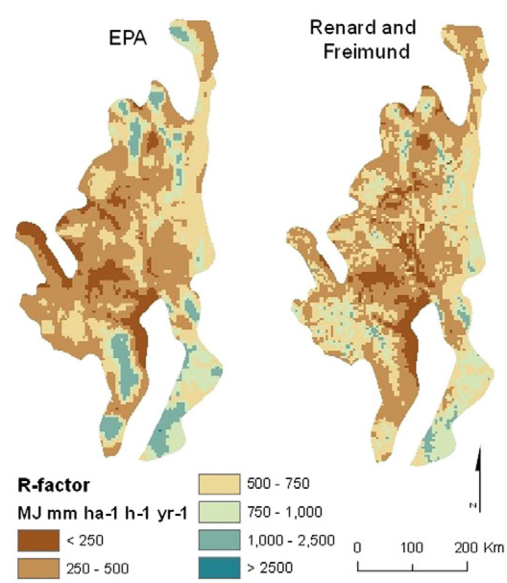

Fig. 5. Historic rainfall erosivity (R-factor) layers from the US Environmental Protection Agency (EPA) and calculated using Eqs. (2a)–(2b) (Renard and Freimund, 1994).

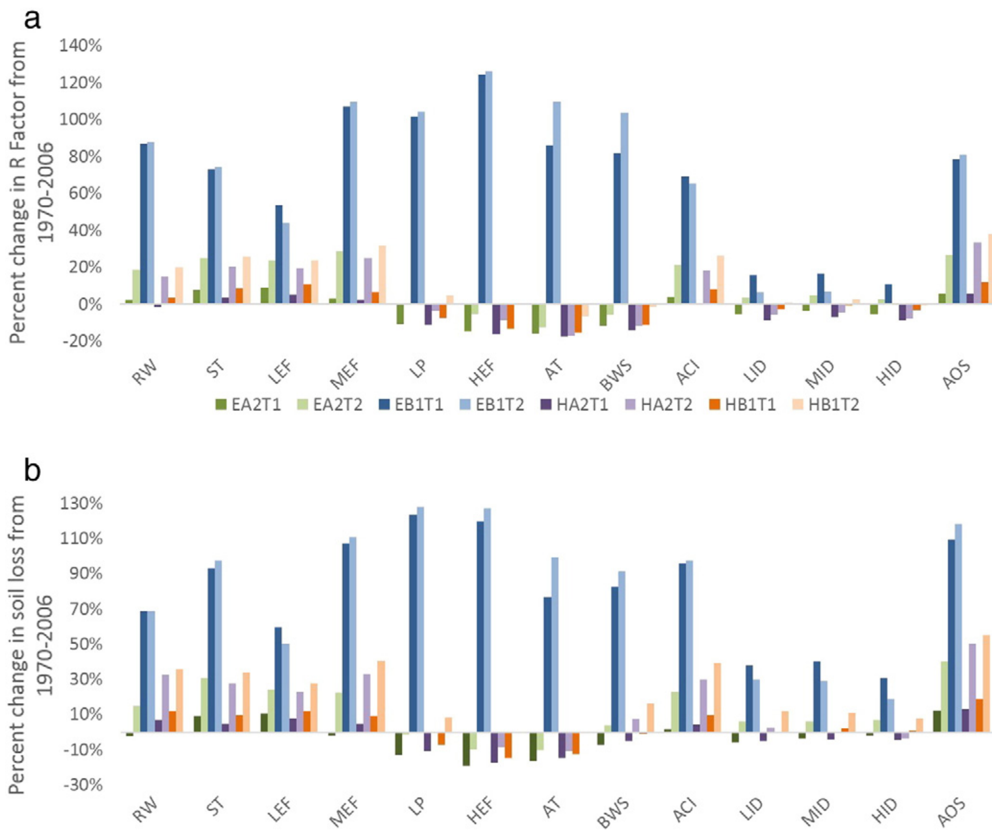

Fig. 6. Change in mean R factor (a) or soil loss (b) for each land cover type calculated using downscaled data from GCM ECHAM5 (E) or HadCM3 (H), climate scenarios A2 and B1, for time periods T1 (2010–2040) and T2 (2041–2070).

4. Results

We first present the new rainfall erosivity layers for the historic time and future combinations. We then present results of the erosion simulations showing how projected soil loss varies by climate model, emission scenario, time period, and the presence or absence of wildfire.

4.1. Rainfall erosivity factor

Rainfall erosivity is the principal factor in RUSLE by which we incorporated climate change into our study. We evaluate our process using a comparison to Nearing (2001) and the rainfall erosivity layer developed by the EPA. Nearing (2001) showed changes ranging from −10% to +10% in rainfall erosivity for the SRE using Renard and Freimund's equation (1994) with climate data used directly from the HadCM3 GCM. In contrast, we found higher changes that ranged from −3% (HadCM3 A2 T1) to 14% (HadCM3 B1 T2). Despite the obvious similarities in GCM data and equations, the differences in estimating rainfall erosivity between our analysis and Nearing's reflect key advances in climate science. The major difference is that Nearing used HadCM3 data at the original scale of 2.5° latitude by 3.75° longitude (about 295 × 278 km at 45° of latitude) compared with the 2 × 2 km downscaled data used here. The coarser scale may have diluted the effect of topography on precipitation, which is critical in this mountainous region. Nearing also did not account for changes in the amounts of precipitation that falls as rain versus snow, as he used average annual precipitation, in contrast to this study which calculated the amount of seasonal rainfall only. The advantage of the method described here is that we were able to use temperature to adjust the rainfall values that directly affect soil loss. Lastly, there was a minor difference in the study years, as Nearing compared the period 2000–2019 to 2080–2099, whereas this study compared the period 1970–2006 to 2010–2040 and 2041–2070 (Nearing, 2001).

Table 6
Percent change in mean future rainfall erosivity from the mean historic rainfall erosivity; all rainfall erosivities were calculated using Renard and Freimund's equation (1994) with a 1 °C threshold to predict hydrologic regime (Cooley et al., 1988).

GCM-scenario	T1	T2
	2010–2040	2041–2070
ECHAM5-A2	1	16
ECHAM5-B1	63	62
HadCM3-A2	−3	10
HadCM3-B1	12	14

The mean values of the historic EPA and RF rainfall erosivity layers (R_{EPA} and R_{RF}, respectively) for the entire SRE are similar, at 492 and 476 MJ mm ha^{-1} h^{-1} yr^{-1} respectively. Similar spatial patterns occur between the EPA and RF rainfall erosivity, particularly throughout central Colorado and around the edge of the San Luis valley (Fig. 5). The coefficients of variation, indicating dispersion of the data around the means, are 60% for the R_{EPA} and 45% for the R_{RF}, suggesting that the R_{RF} does not capture as much of the extreme lowest and highest rainfall intensity as the R_{EPA}. The disparity in capturing extremes may result from the methodological differences; the R_{EPA} was generated as a function of measured rainfall intensity and topographical data while the R_{RF} is a function of mean annual rainfall using a temperature threshold to indicate whether seasonal precipitation fell as rain or snow. It is also likely that the statistically downscaled climate data do not capture the extremes of weather. However, R_{RF} is the best available data for this research, and its use is supported by the generally close match of R_{RF} to

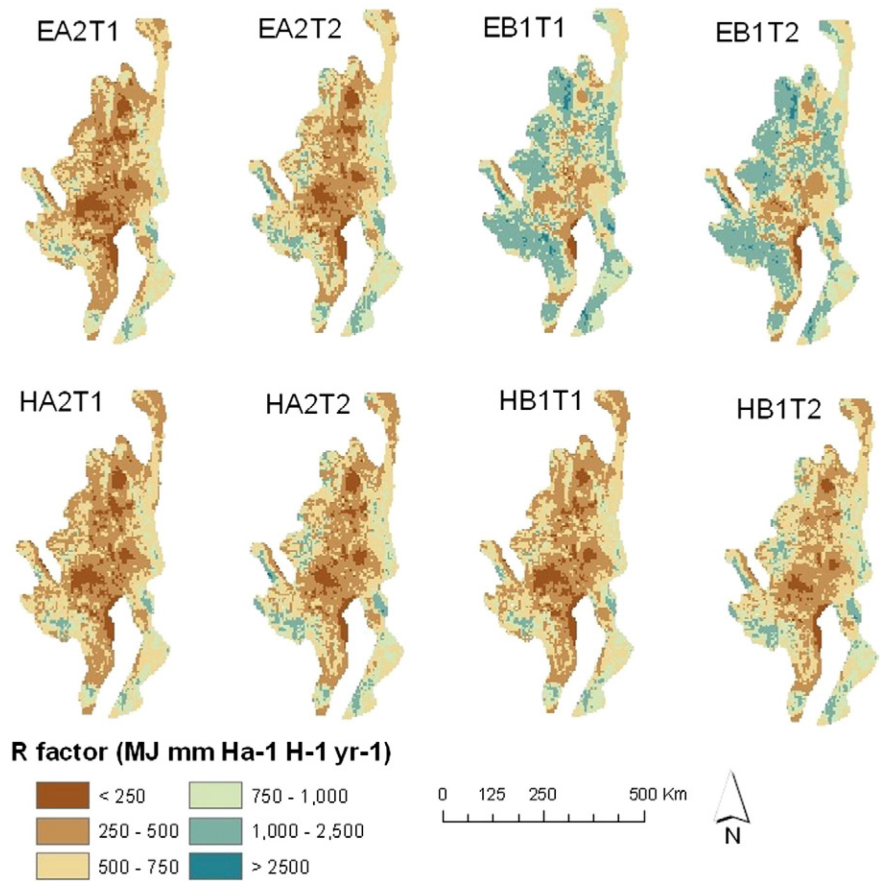

Fig. 7. Rainfall erosivity (R-factor) calculated using Renard and Freimund's equation (1994) for climate predictions using downscaled data from GCMs ECHAM5 (E) and HadCM3(H) for SRES climate change scenarios A2 and B1 and for two time periods (T1 = 2010–2040, T2 = 2041–2070).

R_{EPA}. Based on these comparisons, we concluded that the RF method of estimating rainfall erosivity is suitable for generating rainfall erosivity layers for future climates.

For each of the 13 land cover types modeled (Table 1), the combinations of downscaled ECHAM5 data, climate scenario B1, and time periods T1 or T2 (ECHAM5-B1) result in the largest percent increases above the historic $R_{rf,}$ ranging from an 11% increase for HID to 126% for HEF. High and mid elevation forests show the largest increases in rainfall erosivity, while high elevation forests and alpine tundra show the largest decreases. HadCM3-A2 for time period T1 provided the smallest percent increases or decreases for every land cover type (−18% to 5%) except for AOS where ECHAM5-A2 T1 showed the smallest increase at 5% (Fig. 6a). Future conditions, represented by the scenarios and associated climate projections that we used, resulted in a broad range of changes in soil loss which reflect the current uncertainty about those conditions.

Considering the SRE overall, the B1 scenario generally shows the largest increases in rainfall erosivity for the future climate data versus the historic data, ranging from increases of 62 to 63% for ECHAM5-B1 and 12 to 14% for HadCM3-B1 (Table 6, Fig. 7). Although the RF equation used only mean annual rainfall, the formulation of seasonal hydrologic regime using the 1 °C temperature threshold actually incorporated seasonal differences in temperature and precipitation into the development of rainfall erosivity GIS layers for the historic and future climate. The higher erosivity values with the B1 scenario, versus the A2 scenario, occurred largely because of warmer autumn temperatures with the B1 scenario, which ensured that more precipitation was treated as rain than for the historic layer (Fig. 8).

Rainfall erosivity layers developed for the A2 scenario show larger differences between the first and second future time periods than those developed for the B1 scenario; erosivity increased from 1% to 16% for ECHAM-A2 and from −3% to 10% for HadCM3-A2 (Table 6). The larger increases in erosivity with the A2 scenario result mainly from the greater temperature increases with A2 than with B1, which lead to greater increases in rainfall as mentioned above.

The only projected decrease in rainfall erosivity from the historic time to the future, a change of 3%, occurred with the HadCM3-A2 T1 combination. The low erosivity projection with this combination was most likely due to lower temperature projections, which caused relatively less precipitation to occur as rain; temperatures for the HadCM3-A2 T1 combination were the lowest and second lowest of all combinations during autumn and winter, respectively (Fig. 8).

4.2. Soil loss

For the entire SRE, the estimated average soil loss, across the 100 simulations, for the historic period was 11 Mg ha^{-1} yr^{-1} without wildfire and 12 Mg ha^{-1} yr^{-1} with wildfire (Fig. 9a). To evaluate RUSLE, we compared our overall historic results to those from the EPA Environmental and Monitoring Assessment Program (EMAP). Our estimates (11 and 12 Mg ha^{-1} yr^{-1}) are well within expected modeled values as the EPA EMAP regional scale RUSLE results range from 2 to 17 Mg ha^{-1} yr^{-1} for the SRE using data for 1961–1990.[10] Our estimates are characterized by a strong right skewed distribution, where nearly all of the cells in each soil loss raster have values between 0 and 10 Mg ha^{-1} yr^{-1} but a few cells show much higher values. In agreement with our simulation, Larsen and MacDonald (2007), who conducted a metadata study of nine wildfire field studies in Colorado, show that most of the data points measured between 0 and 10 Mg ha^{-1} yr^{-1} with just a few values between 10 and 100 Mg ha^{-1} yr^{-1}.

[10] http://www.epa.gov/esd/land-sci/emap_west_browser/pages/wemap_mm_sl_rusle_a_khy_qt.htm#mapnav. Accessed 2011.

The estimated mean land cover factor across the cells of the SRE differs little across the 100 iterations with wildfire for the distribution of a given climate/scenario/time period combination (Fig. 9a). As a result, mean soil loss per hectare also varies little across iterations implying that there is little uncertainty in soil loss calculations based on burned area projections. Parallel lines of iteration data indicate that there is no statistical interaction between rainfall erosivity and land cover in the model. However, mean soil loss differs greatly among some of the nine combinations (Fig. 9). The ECHAM5-B1 combination produces the most soil loss, which would be expected from the relatively high rainfall erosivity values for these combinations, while the historic combination produces the least soil loss. The ANOVA summary of soil loss calculated for treatment combinations (GCM, scenario, and time period) and land cover with fire indicate that at least one set of soil loss values is significantly different from the other soil losses (Table 7). The Tukey HSD test shows highly significant differences between GCM/scenario/time period comparisons, with all p-values less than 2.0E − 16 except for the comparison HadCM3-B1 T2 to ECHAM5-A2 T2, which has a significant p-value of 0.001 (not shown). These comparisons are all significantly different in part because the variation within each combination of GCM, scenario, and time period is very small (Fig. 9a).

Among the simulations of the entire SRE without future wildfire (i.e. accounting for climate change only), future soil loss increases over historic soil loss by from 3% for HadCM3-A2 T1 to 60% for ECHAM5-B1 T1 (Fig. 9b). The large increase for the ECHAM5-B1 T1 combination is expected, as rainfall erosivity for ECHAM 5-B1 is consistently higher than it is for other combinations (Fig. 7). Soil loss in time period T2 is also highest with the ECHAM5-B1 GCM/scenario combination. During the autumn, ECHAM5-B1 has the warmest weather, indicating that a greater portion of precipitation falls as rain instead of snow. Further, during the winter months ECHAM5-B1 has the warmest and wettest weather of all the combinations (Fig. 8). In contrast, HadCM3-A2 has the smallest percent increase in erosion over the historic erosion rate, which is likely due to the cooler winter and autumn temperatures, resulting in more of the precipitation falling as snow (Fig. 8).

Including climate change effects only, the largest percent increases in soil loss for each land cover type occur for either ECHAM5-B1 T1 or ECHAM5-B1 T2 (Fig. 6b) which is expected because these two combinations had the largest percent increases in rainfall erosivity for each land cover type (Fig. 6a). The largest increases, each more than double the historic rates of soil loss, are predicted to occur in mid elevation forest (111%), high elevation forest (127%), and lodgepole pine (128%) land cover types. The lowest increases or actual decreases in percent soil loss for each land cover type occurred with the ECHAM5-A2 T1 combination and ranged from − 19% (HEF) to 12% (AOS).

The increases in soil loss due to wildfire (i.e., the differences in soil loss calculated using the C-factor with fire versus the C-factor without fire,) range from 3% (ECHAM5-A2 T1, ECHAM5-B1 T1) to 5% (HadCM3-A2 T2) (Fig. 9b). The mean increase in soil loss due to fire is relatively small compared to the change in soil loss due to climate change because the projected annual increases in burned area due to climate change are relatively small, ranging from 0.32% (HadCM3-A2) to 0.63% (ECHAM-B1) of the SRE (Litschert et al., 2012).

Fig. 10 shows maps of mean annual historic (1970–2006) soil loss (left) and median (out of 100 iterations) rasters of percent change in soil loss from historic for two of the eight combinations, the one with the highest percent increase in soil loss due to climate change and wildfires (ECAHM5-B1 T1, center) and the one with the mid-range percent increase (HadCM3-B1 T2, right); these three rasters also are used to calculate Fig. 11 and Table 8. The historic soil loss ranged mainly from 0 to 100 Mg ha^{-1} yr^{-1} across the SRE; a very few cells, in areas likely to burn at high severity, produced higher values. The lowest soil loss values were typically at the higher elevations. A few cells in EB1T1 and HB1T2 had a percent change in soil loss of greater than 1000%; these areas are visible as dark circles which represent large fires. It is quite likely that these areas pre-fire had very low rates of soil loss and after burning, particularly if they were subjected to a high severity burn, the percent change in erosion rate could be greater than 1000%. For example, an increase from 0.01 Mg ha^{-1} yr^{-1}, to 0.11 Mg ha^{-1} yr^{-1} represents a 1000% increase in soil loss. The HadCM3-B1 T2 combination had a few areas projected to have decreases in soil loss which were generally traced to local decreases in rain erosivity.

Although there is considerable spatial variability in our estimates of soil loss, 83% of the area in the historic raster and 79 to 81% of the area in the ECHAM5-B1 T1 and HadCM3-B1 T2 median rasters produce less than 10 Mg ha^{-1} yr^{-1} (Fig. 11, Table 8). Across the historic raster there is only a 1% likelihood of any cell losing more than 200 Mg ha^{-1} yr^{-1} of soil. In contrast, the likelihood of a cell losing more than 200 Mg ha^{-1} yr^{-1} of soil was doubled for the ECHAM5-B1 T1 raster over the historic erosion raster (Fig. 11, Table 8). Cells losing these large amounts of soil are typically located on steep slopes and at risk for high severity fires. Although 200 Mg ha^{-1} yr^{-1} may seem like a large amount, it is not unprecedented. For example, in a study of soil loss and mountain roads, 200 Mg ha^{-1} of soil was lost in an eight month period from a 165 m^2 site with a native surface road (sandy loam) with a low (5%) gradient (Swift, 1984).

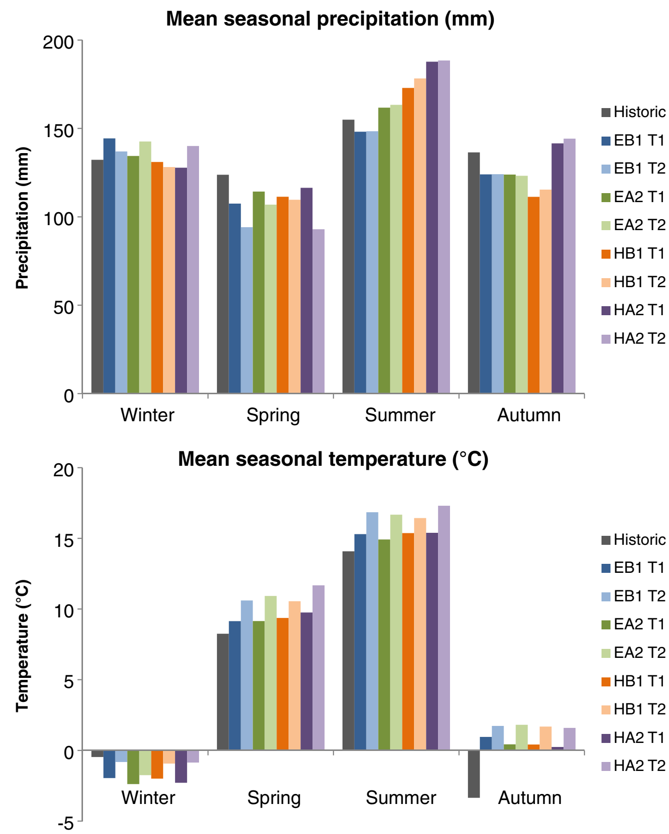

Fig. 8. Mean seasonal precipitation (mm) and mean seasonal temperature (°C) for the SRE using downscaled data from GCMs ECHAM5 (E) and HadCM3(H) for SRES climate change scenarios A2 and B1 and for two time periods (T1 = 2010–2040, T2 = 2041–2070). T1 and T2 values are represented by the darker and lighter shades respectively.

5. Discussion

Two other studies of climate change and erosion have projected substantial increases in erosion at the regional and national scales. Goode et al. (2011) reason that sediment yields in the Northern Rockies are likely to increase by an order of magnitude above 20th century

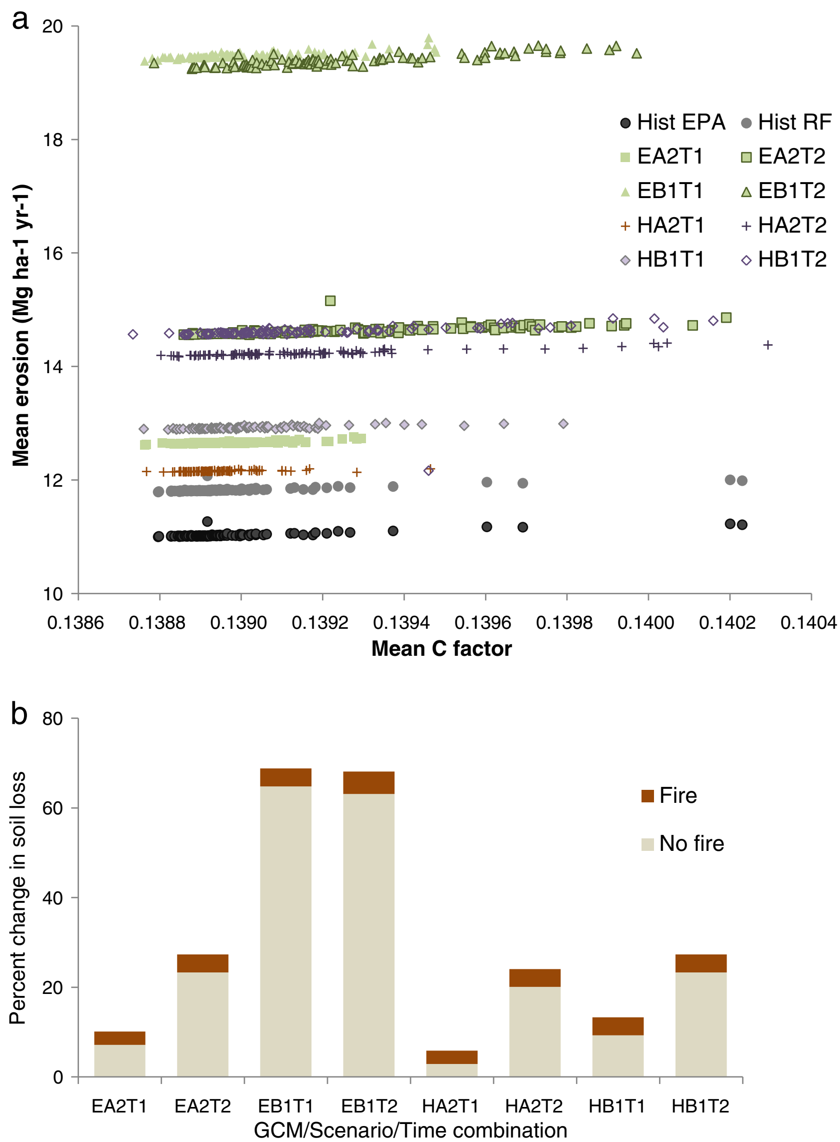

Fig. 9. (a) Mean values for 100 iterations of soil loss due to climate change and fire for historic (Hist) or downscaled data versus to mean land cover (C-factor) and (b) Percent change in soil loss from historic to future combinations with and without fire using data from GCMs ECHAM5 (E) and HadCM3 (H) for climate change scenarios A2 and B1 and for two time periods (T1 = 2010–2040, T2 = 2041–2070).

sediment yields (1.46 Mg ha^{-1} yr^{-1}), which is a much larger increase than the median values found in this study. In contrast, in a review of the effects of climate change on erosion, Nearing et al. (2004) found that erosion is likely to increase by 1.7% based on a 1% increase in precipitation, in U.S. locations where rainfall erosivity increases and for the analysis years described above. In agreement with Nearing et al. for the SRE, we found that average soil loss also was projected to increase by 1.7 times the average increase in rainfall for the seven future combinations that project rainfall increases (rainfall decreases for HadCM3-A2 T1).

At the regional scale, the effects of climate change on chronic soil loss tend to be much greater than the effects of wildfire (Fig. 9b), although wildfire is a critical ecological and geomorphic process in the SRE. Studies conducted at watershed to plot-scales have shown increases of one to three orders of magnitude in runoff and erosion after wildfire (Benavides-Solorio and MacDonald, 2001; DeBano, 2000; Morris and Moses, 1987). Indeed, such increases are apparent in the cumulative frequency plots of the percent change in soil loss due to wildfires (Fig. 11). However, in any given year wildfire it is not likely to cover more than 3% of the SRE (Litschert et al., 2012), such that at the regional scale the effects of wildfire on soil loss are relatively minor.

In this study, estimated soil loss is highest in areas of long steep slopes and highly erodible soils where there is a high likelihood of the forest burning at high severity. Because we stochastically generated

Table 7
ANOVA test summary for differences in soil loss caused by climate change and wildfire (soil loss ~ rainfall erosivity factor (treatment) + land cover factor).

	Degrees of freedom	Sum squares	Mean sq	F value	Pr(>F)
Treatment	9	7901.6	877.95	115464.7	<2.2 E−16
Land cover factor	1	1.5	1.5	197.72	<2.2 E−16
Residuals	989	7.5	0.01		

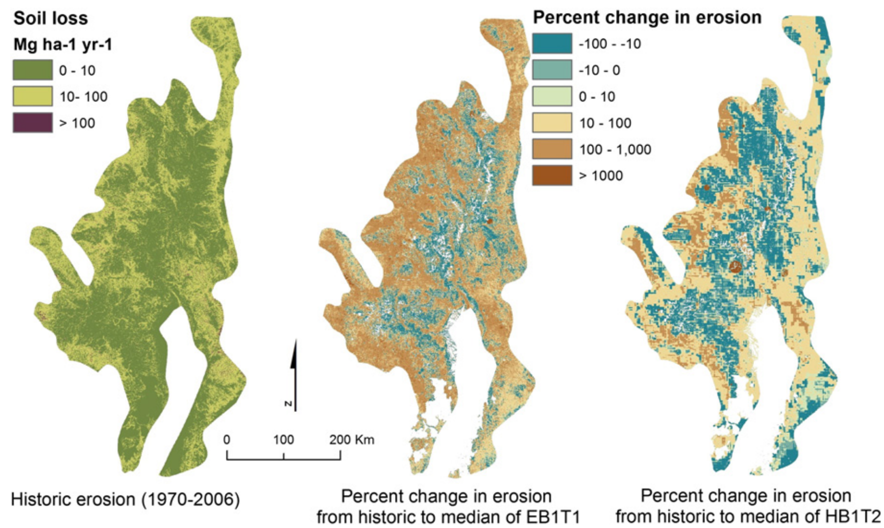

Fig. 10. Historic soil loss (left) and percent change in soil loss due to climate change and wildfire shown for median rasters for simulations using data from downscaled GCM ECHAM5 and climate change scenario B1 (2010–2040) (center) and downscaled GCM HadCM3 and scenario B1 (2041–2070) (right).

wildfires for the entire SRE, we do not identify particular watersheds that would produce certain levels of soil loss; however, we believe that these results can help regional land managers and water planners understand the risks posed by future climate change and wildfire to water supply.

The highest percent increases in soil loss occur in mid and high elevation forest, lodgepole pine, and alpine tundra, which suggests that there will be more potential for soil loss at middle to higher elevations than has happened historically. These soil loss increases may be due to the precipitation phase change to rain at higher elevations as temperatures increase. Smaller percent changes are generally expected in developed areas, which are mostly at lower slope gradients and elevations. The variability of our results reflects the differences in scenarios, time periods, and climate models, but also may reflect continuing uncertainties in our models. Yet, we believe our results will be useful to land managers as indications of the relative changes in soil loss likely for different land cover types, but further research at finer resolution will be useful in local areas.

There are two practical limitations to using RUSLE in the current context. First, RUSLE does not account for mass wasting or gully erosion, which suggests that the soil loss values calculated in this study may underestimate the full potential for erosion. Secondly, RUSLE calculates soil loss on a hillslope, and some of that sediment may not be delivered to the stream downslope. Further, RUSLE may not accurately capture the extremes of soil loss, as Larsen and MacDonald (2007) found that RUSLE tended to over-predict measured values of less than 1 Mg ha^{-1} yr^{-1} and under-predict the highest measured values for postfire sediment yields by an order of magnitude or more. The net effect of these limitations on estimated soil loss and delivery to the stream is unknown and could be either positive or negative.

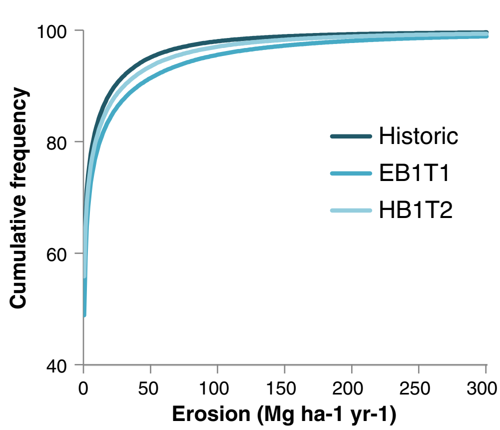

Fig. 11. Cumulative frequency of raster cells with given erosion values for the three GIS layers displayed in Fig. 9.

Factors such as topography, land cover, and soil type affect sediment delivery, and recovery of the land cover is critical. For example, it can take more than five years for sediment yields to return to the normally low rate of undisturbed forest (Benavides-Solorio and MacDonald, 2005; Moody and Martin, 2009; Morris and Moses, 1987; Pietraszek, 2006; Rhoades et al., 2011). In a stochastic study such as this, it is impractical to attempt to track and develop land cover for several years after a fire. Hence, we simulated worst case scenarios by calculating soil loss for the season of the fire only.

We took a broad approach to the problem of climate change, wildfire, and erosion. Further research could help to hone this issue in different ways. First, research conducted at a finer scale will be necessary to understand local impacts in a particular watershed, particularly given the long recovery period required for burned watersheds (Rhoades et al., 2011). Second, improvements in projections of emissions and climate variables will be critical. Our projections of erosivity and thus soil loss differ greatly across the estimates of future temperatures associated with the different emission scenarios and GCMs. Further improvements in climate models will lead to a better quantitative understanding of future temperatures and of the likely extremes in precipitation events which drive erosional processes. Third, inclusion of mass wasting and gullying processes would be a useful addition to this study and would require separate modeling processes. Finally, vegetation change data due to climate change were not available to us, although it is generally agreed that changes will occur. Future research must determine, how changing vegetation will affect the amount of soil losses in combination with climate change.

6. Conclusions

We calculated soil loss using RUSLE to estimate potential effects of climate change and wildfires on soil loss in watersheds important for water supply in the western U.S. The overall mean soil loss is likely to increase over historic levels by from 3% to 60%. The highest amounts of future soil loss were calculated for all vegetation types with climate simulated by the ECHAM5 GCM for the B1 emission (IPCC, 2007). Lodgepole pine experienced the largest soil loss projections among the vegetation types at 128%. The direct effects of climate change on precipitation and erosivity, not increases in wildfire, account for nearly all of

Table 8
Likelihood of soil loss due to climate change and wildfire for three median value rasters in selected combinations: Historic, and using downscaled data from EB1T1 = GCM ECHAM5 and climate change scenario B1 (2010–2040), and HB1T2 = GCM HadCM3 and scenario B1 (2041–2070). The tables show the very slight differences between the simulations with and without wildfire and climate change.

Soil (Mg ha^{-1} yr^{-1})	Wildfire and climate change			Climate change only		
	Historic	EB1T1	HB1T2	Historic	EB1T1	HB1T2
>1	33%	41%	35%	33%	40%	35%
>10	17%	21%	19%	16%	8%	18%
>50	100%	100%	100%	100%	100%	100%
>100	2.0%	4.4%	2.9%	1.9%	1.7%	2.8%
>200	0.7%	1.9%	1.1%	0.7%	1.0%	0.6%

the increase in soil loss. The lowest overall increase in soil loss, 3%, was found with the HadCM3 GCM and A2 scenario. At this scenario–GCM combination, several land cover types (i.e., lodgepole pine, alpine tundra, and developed areas) showed a decrease in soil loss with high elevation forest indicating the largest projected decrease at 19%. The additional effects of increases in wildfire on soil loss range from 3% to 5% across all scenario–GCM combinations. The wide range in estimates of future soil loss across the combinations reflect the range in projections of climatic change, and are a reminder of the great uncertainty that remains about our future climate; although temperature increases are expected the degree of increase is impossible to estimate precisely, and precipitation changes are even less clear-cut.

Although most areas in both historic and future simulations show soil losses of less than 1 Mg ha^{-1} yr^{-1}, the likelihood of local soil losses of above 100 Mg ha^{-1} yr^{-1} may double in some areas in the future. Based on these findings, we suggest that land managers should anticipate increased chronic soil loss due first of all to the direct effects of climate change and secondly due to a climate-induced increase in wildfire. More detailed study of local risk-based effects of wildfire is recommended.

Acknowledgments

This research was supported by funds from the Rocky Mountain Research Station (RMRS), U.S. Forest Service. The authors thank Scott Baggett of the RMRS for his statistical guidance. We also thank three anonymous reviewers for their careful attention and suggestions that improved this manuscript.

References

R. Development Core Team, 2011. R: A Language and Environment for Statistical Computing R Foundation for Statistical Computing, Austria, Vienna.
Aashto, 2004. A Policy on Geometric Design of Highways and Streets. American Association of State Highway and Transportation Officials (872 pp.).
Bailey, R.G., Avers, P.E., King, T., McNab, W.H., 1994. Ecoregions and subregions of the United States (map) 1:7,500,000 (with supplementary table of map unit descriptions, compiled and edited by W. H. McNab and R. G. Bailey) Washington, DC: U. S. Forest Service.
Balshi, M.S., Mcguire, A.D., Duffy, P., Flannigan, M., Walsh, J., Melillo, J., 2009. Assessing the response of area burned to changing climate in western boreal North America using a Multivariate Adaptive Regression Splines (MARS) approach. Glob. Chang. Biol. 15, 578–600. http://dx.doi.org/10.1111/j1365-2486200801679x.
Barnett, T.P., Adam, J.C., Lettenmaier, D.P., 2005. Potential impacts of a warming climate on water availability in snow-dominated regions. Nature 438, 303–309. http://dx.doi.org/10.1038/nature04141.
Bartlein, P.J., Hostetler, S.W., Shafer, S.L., Holman, J.O., Solomon, A.M., 2003. The seasonal cycle of wildfire and climate in the western United States. 5th Symposium on Fire and Meteorology American Meteorological Society, Orlando, FL, pp. 39-1–39-6.
Benavides-Solorio, J., MacDonald, L.H., 2001. Post-fire runoff and erosion from simulated rainfall on small plots, Colorado Front Range. Hydrological Processes 15, 2931–2952.
Benavides-Solorio, J., MacDonald, L.H., 2005. Measurement and prediction of postfire erosion at the hillslope scale. Colorado Front Range. Int. J. Wildland Fire 14, 1–18.
Breiby, T., 2006. Assessment of soil erosion risk within a subwatershed using GIS and RUSLE with a comparative analysis of the use of STATSGO and SSURGO soil databases. Papers in Resource Analysis, vol. 8. Saint Mary's University of Minnesota Central Services Press, Winona, MN (22 pp.).
Brown, T.C., Hobbins, M.T., Ramirez, J.A., 2008. Spatial distribution of water supply in the coterminous United States. J. Am. Water Resour. Assoc. 44, 1474–1487. http://dx.doi.org/10.1111/j.1752-1688.2008.00252.x.
Caminiti, J.E., 2004. Catchment modelling—a resource manager's perspective. Environ. Model Softw. 19 (11), 991–996.
Cañon, J., González, J., Valdéz, J., 2007. Precipitation in the Colorado River Basin and its low frequency associations with PDO and ENSO signals. J. Hydrol. 333, 252–264.
Cañon, J., Dominguez, F., Valdéz, J.B., 2011. Downscaling climate variability associated with quasi-periodic climate signals: a new statistical approach using MSSA. J. Hydrol. 398 (1–2), 65–75 (509).
Cooley, K.R., Hanson, C.L., Johnson, C.W., 1988. Precipitation erosivity index estimates in cold climates. Trans. ASAE 31, 1445–1450.
Daly, C., Neilson, R.P., Phillips, D.L., 1994. A statistical-topographic model for mapping climatological precipitation over mountainous terrain. J. Appl. Meteorol. 33, 140–160.
Dawen, Y., Shinjiro, K., Tailkan, O., Toshio, K., Katumi, M., 2003. Global potential soil erosion with reference to land use and climate changes. Hydrol. Process. 17, 2913–2928.
DeBano, L., 1981. Water repellent soils: a state of the art. USDA Forest Service GTR-PSW-046, Berkeley, California (21 pp.).
DeBano, L., 2000. The role of fire and soil heating on water repellency in wildland environments: a review. J. Hydrol. 231–232, 195–206.
Dominguez, F., Cañon, J., Valdéz, J., 2010. IPCC-AR4 climate simulations for the Southwestern US: the importance of future ENSO projections. Clim. Change 99, 499–514.
Drever, C.R., Bergeron, Y., Drever, M.C., Flannigan, M., Logan, T., Messier, C., 2009. Effects of climate change on occurrence and size of large fire in a northern hardwood landscape: historical trends, forecasts, and implications for climate change in Temiscamingue, Quebec. Appl. Veg. Sci. 12, 261–272.
Dunne, T., Leopold, L., 1978. Water in Environmental Planning. W. H. Freeman & Company, San Francisco, CA (818 pp.).
EPA (US Environmental ProtectionAgency), 2000. National water quality inventory. 1998 Report to Congress. Environmental Protection Agency, Washington, DC.
Feng, S., Hu, Q., 2007. Changes in winter snowfall/precipitation ratio in the contiguous United States. J. Geophys. Res. 112, D15109. http://dx.doi.org/10.1029/2007JD008397.
Foster, G.R., Meyer, L.D., 1977. Soil erosion and sedimentation by water: an overview. Proc. Natl. Symp. on Erosion and Sedimentation by Water, Chicago, IL. Am. Soc. Agric. Eng., St. Joseph, MI, pp. 1–13.
Gonzalez-Bonorino, G., Osterkamp, W.R., 2004. Applying RUSLE 20 on burned-forest lands: an appraisal. J. Soil Water Conserv. 59 (1), 36–42.
Goode, J.A., Luce, C.H., Buffington, J.M., 2011. Enhanced sediment delivery in a changing climate in semi-arid mountain basins: implications for water resource management and aquatic habitat in the Northern Rocky Mountains. Geomorphology. http://dx.doi.org/10.1016/j.geomorph.2011.06.021.
Graham, R.T. (Ed.), 2003. Hayman Fire Case Study. General Technical Report RMRSGTR-114. Rocky Mountain Research Station, US Forest Service, Ogden, UT.
Guobin, T., Shulin, C., Donald, M.K., 2006. Modeling the impacts of no-till practice on soil erosion and sediment yield with RUSLE, SEDD, and ArcView GIS. Soil Tillage Res. 85, 38–49.
Haan, C.T., Barfield, B.J., Hayes, J.C., 1994. Design Hydrology and Sedimentology for Small Catchments. Academic Press, San Diego, CA (588 pp.).
Hay, L.E., Wilby, R.L., Leavesley, G.H., 2000. A comparison of delta change and downscaled GCM scenarios for three mountainous basins in the United States. J. Am. Water Res. Assoc. 36 (2), 387–397.
Huffman, E.L., MacDonald, L.H., Stednick, J.D., 2001. Strength and persistence of fire-induced soil hydrophobicity under ponderosa and lodgepole pine, Colorado Front Range. Hydrol. Process. 15, 2877–2892.
IPCC, 2007. Climate Change 2007: Synthesis Report. In: Core Writing Team, Pachauri, R.K., Reisinger, A. (Eds.), Contribution of Working Groups I, II and III to the Fourth Assessment Report of the Intergovernmental Panel on Climate Change. IPCC, Geneva, Switzerland (104 pp.).
Israelson, C.E., Clyde, C.G., Fletcher, J.E., Israelson, E.K., Haws, F.P., Parker, P.E., Farmer, E.E., 1980. Erosion control during highway construction: Manual on principles and practices report 221. Transportation Research Board, National Research Council, Washington, DC.
Kilgore, B., 1981. Fire in ecosystem distribution and structure: western forests and scrublands. In: Mooney, H.A., Bonnicksen, T.M., Christensen, N.L. (Eds.), Proceedings of the Conference: Fire Regimes and Ecosystem Properties. General Technical Report WO-GTR-26. US Forest Service, pp. 58–89.
LandFire, 2006. The National Map LANDFIRE: LANDFIRE National Existing Vegetation Type layer In U S Department of Interior, Geological Survey.
Larsen, I.J., MacDonald, L.H., 2007. Predicting postfire sediment yields at the hillslope scale: testing RUSLE and disturbed WEPP. Water Resour. Res. 43, W11412. http://dx.doi.org/10.1029/2006WR005560.
Larsen, I.J., MacDonald, L.H., Brown, E., Rough, D., Welsh, M.J., Pietraszek, J.H., Libohova, Z., Benavides-Solorio, J.D., Shaffrath, K., 2009. Causes of post-fire runoff and erosion: water repellency, cover, or soil sealing? Soil Sci. Soc. Am. 73, 1393–1407.

Litschert, S.E., Brown, T.C., Theobald, D.M., 2012. Historic and future wildfire extent in the Southern Rockies Ecoregion Forest Ecology and Management. For. Ecol. Manag. 268, 124–133. http://dx.doi.org/10.1016/jforeco201112024.
Littell, J.S., McKenzie, D., Peterson, D.L., Westerling, A.J., 2009. Climate and wildfire are burned in western US ecoprovinces, 1916–2003. Ecol. Appl. 19 (4), 1003–1021.
MacDonald, L.H., Stednick, J.D., 2003. Forests and water: a state-of-the-art review for Colorado CWRRI Completion Report No 196. Colorado State University, Fort Collins, Colorado (65 pp.).
McCool, D.K., Brown, L.C., Foster, G.R., Mutchler, C.K., Meyer, L.D., 1987. Revised slope steepness factor for the Universal Soil Loss Equation. Trans. ASAE 30 (5), 1387–1396.
McCuen, R.H., 1998. Hydrologic Analysis and Design, second ed. Prentice-Hall, Inc., Upper Saddle River, New Jersey (07458).
Merritt, W.S., Letcher, R.A., Jakeman, A.J., 2003. A review of erosion and sediment transport models. Environ. Model Softw. 18 (8–9), 761–799.
Miller, J.D., Nyhan, J.W., Yool, S.R., 2003. Modeling potential erosion due to the Cerro Grande Fire with a GIS-based implementation of the Revised Universal Soil Loss Equation. Int. J. Wildland Fire 12, 85–100.
Moody, J.A., Martin, D.A., 2001. Initial hydrologic and geomorphic response following a wildfire in the Colorado Front Range. Earth Surf. Process. Landf. 26, 1049–1070.
Moody, J.A., Martin, D.A., 2009. Synthesis of sediment yields after wildland fire in different rainfall regimes in the western United States. Int. J. Wildland Fire 18, 96–115. http://dx.doi.org/10.1071/WF07162.
Morris, S.E., Moses, T.A., 1987. Forest fire and the natural soil erosion regime in the Colorado front range. Ann. Assoc. Am. Geogr. 77 (2), 245–254.
Nayak, A., Marks, D., Chandler, D.G., Seyfried, M., 2010. Long-term snow, climate, and streamflow trends at the Reynolds Creek Experimental Watershed, Owyhee Mountains, Idaho, United States. Water Resources Research 46, W06519. http://dx.doi.org/10.1029/2008WR007525.
Nearing, M.A., 1997. A single continuous function for slope steepness influence on soil loss. Soil Sci. Soc. Am. J. 61 (3), 917–919.
Nearing, M.A., 2001. Potential changes in rainfall erosivity in the US with climate change during the 21st century. J. Soil Water Conserv. 56 (3), 229–232.
Nearing, M.A., Pruski, F.F., O'Neal, M.R., 2004. Expected climate change impacts on soil erosion rates: a review. J. Soil Water Conserv. 59 (1), 43–50.
Wildland fire in ecosystems: effects of fire on soils and water. In: Neary, D.G., Ryan, K.C., DeBano, L.F. (Eds.), General Technical Report RMRS-GTR-42-volume 4. USDA Forest Service, Rocky Mountain Research Station, Ogden, UT (250 pp.).
Nijssen, B., O'Donnell, G.M., Hamlet, A.F., Lettenmaier, D.P., 2001. Hydrologic sensitivity of global rivers to climate change. Clim. Chang. 50 (143–175), 2001.
Ott, R.L., Longnecker, M., 2001. An Introduction to Statistical Methods and Data Analysis. Duxbury, Pacific Grove, CA (1152 pp.).
Palmieri, A., Shah, F., Dinar, A., 2001. Economics of reservoir sedimentation and sustainable management of dams. J. Environ. Manage. 61, 149–163.
Pietraszek, J.H., 2006. Controls on Postfire Erosion at the Hillslope Scale, Colorado Front Range. (Thesis) Colorado State University, Fort Collins, CO (131 pp.).
Ray, A.J., Barsugli, J.J., Averyt, K.B., 2008. Climate Change in Colorado: A Synthesis to Support Water Resources Management and Adaptation. Western Water Assessment, University of Colorado, Boulder (58 pp.).
Renard, K.G., Freimund, J.R., 1994. Using monthly precipitation data to estimate the R-factor in the revised USLE. J. Hydrol. 157, 287–306.
Renard, K.G., Foster, G.R., Weesies, G.A., McCool, D.K., Yoder, D.C., 1997. Agric Handbook 703 USDA, Washington, DC (404 pp.).
Rhoades, C.C., Entwistle, D., Butler, D., 2011. The influence of wildfire extent and severity on streamwater chemistry, sediment, and temperature following the Hayman Fire, Colorado. Int. J. Wildland Fire 20, 430–442.
Robichaud, P.R., 2000. Fire effects on infiltration rates after prescribed fire in northern Rocky Mountain forests, USA. J. Hydrol. 231–232, 220–229.
Shaw, E.A., Richardson, J.S., 2001. Direct and indirect effects of sediment pulse duration on stream invertebrate assemblages and rainbow trout (*Onchorhynchus mykiss*) growth and survival. Can. J. Fish. Aquat. Sci. 58, 2213–2221.
Spracklen, D.V., Mickley, L.J., Logan, J.A., Hudman, R.C., Yevich, R., Flannigan, M.D., Westerling, A.J., 2009. Impacts of climate change from 2000 to 2050 on wildfire activity and carbonaceous aerosol concentrations in the western United States. J. Geophys. Res. 114, D20301. http://dx.doi.org/10.1029/2008JD010966.
Swift, L.W., 1984. Gravel and grass surfacing reduces soil loss from mountain road. For. Sci. 30 (3), 657–670.
Toy, T.J., Foster, G.R., 1998. Guidelines for the use of the revised universal soil loss equation (RUSLE) version 106 on mined lands, construction sites, and reclaimed lands. Western Regional Coordinating Center, Office of Surface Mining, Denver, CO (148 pp.).
Troendle, C.A., Olsen, W.K., 1994. Potential effects of timber harvest and water management of streamflow dynamics and sediment transport. In: Covington, W.W., DeBano, L. (Eds.), Sustainable Ecological Systems. 1993 July 12–15; Flagstaff, AZ/USA Gen Tech Rep RM-247. US Department of Agriculture, Forest Service, Rocky Mountain Forest and Range Experimental Station, Fort Collins, CO/USA, pp. 34–41.
Westerling, A.L., Hidalgo, H.G., Cayan, D.R., Swetnam, T.W., 2006. Warming and earlier spring increases western US forest wildfire activity. Science 313, 940–943.
Winchell, M.F., Jackson, S.H., Wadley, A.M., Srinivasan, R., 2008. Extension and validation of a geographic information system-based method for calculating the Revised Universal Soil Loss Equation length-slope factor for erosion risk assessments in large watersheds. J. Soil Water Conserv. 63 (3), 105–111.
Wischmeier, W.H., Smith, D.D., 1978. Predicting rainfall erosion losses. Agriculture Handbook, 537. U. S. Dept Agr., Washington D.C.(58 pp.).
Wood, A.W., Leung, L.R., Sridhar, V., Lettenmaier, D.P., 2004. Hydrologic implications of dynamical and statistical approaches to downscaling climate model outputs. Clim. Chang. 62, 189–216.